J|A|C|S
ARTICLES
Published on Web 03/29/2007

One-Dimensional Supramolecular Organization of Single-Molecule Magnets

Lollita Lecren,[†] Wolfgang Wernsdorfer,[‡] Yang-Guang Li,[†,⊥] Alessandro Vindigni,[§] Hitoshi Miyasaka,[||] and Rodolphe Clérac[†,*]

Contribution from the Université Bordeaux 1, CNRS, Centre de Recherche Paul Pascal - UPR8641, 115 avenue du Dr. Albert Schweitzer, 33600 Pessac, France, CNRS, Institut Néel, BP 166, 25 av. des Martyrs, 38042 Grenoble, France, Laboratorium für Festkörperphysik, Wolfgang-Pauli-Strasse 16 ETH Hönggerberg, CH-8093, Zürich Switzerland. Department of Chemistry, Graduate School of Science, Tohoku University, 6-3 Aramaki-Aza-Aoba, Aoba-ku, Sendai, Miyagi 980-8578, Japan, and CREST, Japan Science and Technology Agency (JST), 4-1-8 Honcho Kawaguchi, Saitama 332-0012, Japan

Received November 6, 2006; E-mail: clerac@crpp-bordeaux.cnrs.fr

Abstract: An out-of-plane dimeric Mn^{III} quadridentate Schiff-base compound, $[Mn_2(salpn)_2(H_2O)_2](ClO_4)_2$ ($salpn^{2-}$ = *N,N′*-(propane)bis(salicylideneiminate)), has been synthesized and structurally characterized. The crystal structure reveals that the $[Mn_2(salpn)_2(H_2O)_2]^{2+}$ units are linked through weak H-bonds ($OH_{water}\cdots O_{Ph}$) in one dimension along the *c*-axis, forming supramolecular chains. The exchange interaction between Mn^{III} ions via the biphenolate bridge is ferromagnetic ($J/k_B = +1.8$ K), inducing an $S_T = 4$ ground state. This dinuclear unit possesses uni-axial anisotropy observed in the out-of-plane direction with $D_{Mn2}/k_B = -1.65$ K. At low temperatures, this complex exhibits slow relaxation of its magnetization in agreement with a *single-molecule magnet* (*SMM*) behavior. Interestingly, the intermolecular magnetic interactions along the one-dimensional organization, albeit weak ($J'/k_B = -0.03$ K), influence significantly the thermally activated and quantum dynamics of this complex. Thus, unique features such as *M* vs *H* data with multiple steps, hysteresis effects, and peculiar relaxation time have been explained considering *SMMs* in small exchange-field perturbations and finite-size effects intrinsic to the chain arrangement. The magnetic properties of this new complex can be regarded as an intermediate behavior between *SMM* and *single-chain magnet* (*SCM*) properties.

Introduction

In the early 1990s, the discovery of magnetization slow relaxation in molecular complexes, called *single-molecule magnets* (*SMMs*), created a flourishing research field at the frontier of physics and chemistry.[1,2] The ultimate ambition of this research activity is to modulate the quantum properties of these nanosized magnets in order (i) to store and to address a large amount of information in specialized devices or (ii) to provide basic components for future quantum computers.[3] More recently, a similar magnetic behavior has been experimentally observed in one-dimensional (1D) arrangements of magnetically coupled anisotropic transition metal ions, called *single-chain magnets* (*SCMs*)[4,5] that are able to keep magnet-type properties at higher temperatures than *SMMs*.[5b,6] At the borderline between these two systems, chemists have developed original systems introducing magnetic interactions between *SMMs* used indeed as building-blocks. Original magnetic properties have been observed such as *SCM* behavior,[7] ferrimagnetism,[8] canted antiferromagnetism,[9] two-dimensional and three-dimensional (3D) correlated *SMM*-type behavior,[9,10] and magnetization slow relaxation induced by finite-size effects in antiferromagnetic 1D systems.[11] The inspiration of all these works is found in the

[†] Université Bordeaux 1; CNRS, Centre de Recherche Paul Pascal UPR8641.
[‡] Institut Néel.
[§] Laboratorium für Festkörperphysik.
[||] Tohoku University and CREST-JST.
[⊥] Present address. Faculty of Chemistry, Northeast Normal University, Changchun, 130024, China.

(1) Reviews: Christou, G.; Gatteschi, D.; Hendrickson, D. N.; Sessoli, R. *MRS Bull.* **2000**, *25*, 66−71. Gatteshi, D.; Sessoli, R. *Angew. Chem., Int. Ed.* **2003**, *42*, 268−297; *Angew. Chem.* **2003**, *115*, 278−309.
(2) (a) Boyd, P. D. W.; Li, Q.; Vincent, J. B.; Folting, K.; Chang, H.-R.; Streib, W. E.; Huffman, J. C.; Christou, G.; Hendrickson, D. N. *J. Am. Chem. Soc.* **1988**, *110*, 8537−8540. (b) Caneschi, A.; Gatteschi, D.; Sessoli, R. *J. Am. Chem. Soc.* **1991**, *113*, 5873−5874. (c) Sessoli, R.; Tsai, H. -L.; Schake, A. R.; Wang, S.; Vincent, J. B.; Folting, K.; Gatteschi, D.; Christou, G.; Hendrickson, D. N. *J. Am. Chem. Soc.* **1993**, *115*, 1804−1816.
(3) (a) Wernsdorfer, W.; Sessoli, R. *Science* 1**999**, *284*, 133−135. (b) Leuenberger, M. N.; Loss, D. *Nature* **2001**, *410*, 789−793.
(4) For review see: Coulon, C.; Miyasaka, H.; Clérac, R. *Struct. Bond.* **2006**, *122*, 163−206.
(5) (a) Caneschi, A.; Gatteschi, D.; Lalioti, N.; Sangregorio, C.; Sessoli, R.; Venturi, G.; Vindigni, A.; Rettori, A.; Pini, M. G.; Novak, M. A. *Angew. Chem., Int. Ed.* **2001**, *40*, 1760; *Angew. Chem.* **2001**, *113*, 1810−1813. (b) Clérac, R.; Miyasaka, H.; Yamashita, M.; Coulon, C. *J. Am .Chem. Soc.* **2002**, *124*, 12837−12844.
(6) Coulon, C.; Clérac, R.; Lecren, L.; Wernsdorfer, W.; Miyasaka, H. *Phys. Rev. B* **2004**, *69*, 132408.
(7) Ferbinteanu, M.; Miyasaka, H.; Wernsdorfer, W.; Nakata, K.; Sugiura, K.; Yamashita, M.; Coulon, C.; Clérac, R. *J. Am. Chem. Soc.* **2005**, *127*, 3090−3099.
(8) Miyasaka, H.; Nakata, K.; Sugiura, K.; Yamashita, M.; Clérac, R. *Angew. Chem., Int. Ed.* **2004**, *43*, 707−711; *Angew. Chem.* **2004**, *116*, 725−729.
(9) Miyasaka, H.; Nakata, K.; Lecren, L.; Coulon, C.; Nakazawa, Y.; Fujisaki, T.; Sugiura, K.; Yamashita, M.; Clérac, R. *J. Am. Chem. Soc.* **2006**, *128*, 3770−3783.

Scheme 1. salpn^{2-}: *N,N′*-(propane)bis(salicylideneiminate), (b) salen^{2-}: *N,N′*-(ethylene)bis(salicylideneiminate), (c) saltmen^{2-}: *N,N′*-(1,1,2,2-tetramethylethylene)bis(salicylideneiminate)

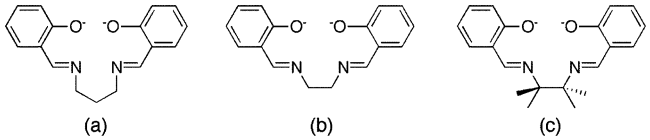

(a) (b) (c)

pioneering works of W. Wernsdorfer and G. Christou who have studied supramolecular dimers and 3D networks of *SMMs*.[12] They have shown that the magnetic interactions were able to tune the dynamics of the original *SMM* unit including the quantum tunneling of the magnetization (*QTM*).[12] This breakthrough oriented our research projects toward the synthesis of covalent and supramolecular networks of *SMMs*.[8−11]

In order to design such systems, the choice of the *SMM* building block is an important step that was guided by the need of simplicity in terms of its molecular structure, its magnetic properties, and its affinity to be connected in networks. On the basis of these requirements, we decided to organize Mn^{III}/salen-type dinuclear *SMMs* into coordination networks and supramolecular organizations in order to probe the influence of a given arrangement on the *SMM* properties of this building unit.[7,13] So far, numerous manganese complexes based on salen-type ligands (H_2salen = *N,N′*-(ethylene)bis(salicylideneimine); Scheme 1) are known, but it was only in 2004 that our group reported on the *SMM* behavior of a dinuclear Mn^{III}/saltmen species: $[Mn_2(saltmen)_2(ReO_4)_2]$ (H_2saltmen = *N,N′*-(1,1,2,2-tetramethylethylene)bis(salicylideneimine); Scheme 1) (**1**).[14] More recently, similar properties have been reported in related complexes: $[Mn_2(saltmen)_2(X)_2]$($X^- = CH_3COO^-, N_3^-$), $[Mn_2(salen)_2(NCO)_2]$ and $[Mn_2(3,5\text{-Brsalen})_2(3,5\text{-Brsalicylaldehyde})_2]$ ($H_2$3,5-Brsalen = *N,N′*-(ethylene)bis(3,5-dibromosalicylideneimine)).[15] In this line, we have recently investigated this type of Mn^{III} complexes with different Schiff-base ligands in order to replace the saltmen^{2-} ligand used in **1** and to analyze the influence of this substitution on the magnetic properties. The *N,N′*-(propane)-bis(salicylideneiminate) ligand (= salpn^{2-}; Scheme 1) has been one of our selected Schiff-base ligands as it can form dinuclear complexes with Mn^{III} ions as exemplified by $[Mn_2(salpn)_2(NCS)_2]$.[16] Nevertheless, the magnetic properties of this dinuclear complex do not reveal the presence of *SMM* behavior.[16]

Herein, we report an example of 1D supramolecular organization of *SMMs*, $[Mn_2(salpn)_2(H_2O)_2](ClO_4)_2$ (**3**), and the detailed studies of its peculiar static and dynamic magnetic properties. This compound possesses a hydrogen-bonded chain structure similar to the one observed in $[Mn_2(saltmen)_2(H_2O)_2](ClO_4)_2$ (**2**). While **2** does not display a *SMM* behavior but an antiferromagnetic order below 5 K induced by significant interchain magnetic interactions,[17] the present compound exhibits an exchange-bias *SMM* behavior characteristically induced by the 1D arrangement of the $[Mn_2(salpn)_2(H_2O)_2]^{2+}$ units. This work illustrates how a fine-tune of the quantum properties required for future applications can be obtained by introducing weak inter-*SMM* antiferromagnetic interactions in a controlled *SMM* spatial organization.

Experimental Section

Synthesis of $[Mn_2(salpn)_2(H_2O)_2](ClO_4)_2$ (3). **3** has already been synthesized by starting from the air-oxidation of $Mn^{II}(ClO_4)_2 \cdot 6H_2O$ in a MeOH/EtOH solution.[18] In the present work, this synthetic approach was improved by using a method already reported for other salen-type ligands[14,17] in order to obtain good single crystals suitable for single-crystal X-ray diffraction. A MeOH solution (20 mL) of $Mn(O_2CCH_3)_3 \cdot 4H_2O$ (1.34 g, 5 mmol) was added to a 50-mL methanol solution of H_2salpn (1.41 g, 5 mmol). The dark-brown solution was then heated at 50 °C and stirred for 30 min. Just before filtration, $NaClO_4$ (solid, 0.61 g, 5 mmol) in 80 mL of water was added to the hot solution. The filtrate was left to stand for one week at 25 °C to form green needle crystals that were collected by a suction filtration, washed with a minimum amount of MeOH, and dried in air (yield: 75% based on Mn precursor). Elemental analysis (%) calcd for $C_{34}H_{36}N_4O_{14}Cl_2Mn_2$: C 45.10, H 4.00, N 6.19, Cl 7.83; found: C 44.77, H 4.01, N 6.18, Cl 7.83; selected IR data (KBr pellet, cm^{-1}): 3375 (br), 3227 (br), 3194 (br), 2950 (w), 1611 (br, ν(C=N)), 1550 (br), 1470 (s), 1444 (m), 1405 (s), 1366 (w), 1344 (w), 1294 (m), 1267 (m), 1216 (s), 1127 (br, ν(Cl−O)), 1100 (br, ν(Cl−O)), 1072 (br, ν(Cl−O)), 963 (s), 943 (w), 926 (w), 897 (s), 856 (s), 750 (m), 623 (m), 536 (w), 503 (w), 446 (s). ***Caution:*** Although we have not experienced any problems in this work, perchlorate salts may be explosive and should be handled with great care.

Physical Measurements. Elemental analyses (C, H, and N) were measured by Service Central d'Analyse of CNRS. IR spectra were recorded in the range 400−4000 cm^{-1} on a Nicolet 750 Magna-IR spectrometer using a KBr pellet. Magnetic susceptibility measurements were performed with a Quantum Design SQUID magnetometer (MPMS-XL). Dc measurements were conducted from 1.8 to 300 K and from −70 kOe to 70 kOe. Ac measurements were performed at frequencies ranging from 0.1 to 1500 Hz with an ac field amplitude of 3 Oe and no applied dc field. The measurements were performed on polycrystalline samples (embedded in grease in order to avoid field-induced reorientation of the microcrystals) of **3**. Experimental data were also corrected for the sample holder and for the sample's diamagnetic contribution calculated from Pascal constants.[19] Magnetization measurements on single crystals were performed with an array of μ-SQUIDs.[20] This magnetometer works in the temperature range of 0.04−7 K and in fields of up to 1.4 T with sweeping rates as high as 10 $T \cdot s^{-1}$, along with a field stability of μT. The time resolution is approximately 1 ms. The field can be applied in any direction of the μ-SQUID plane with precision much better than 0.1° by separately driving three orthogonal coils. In order to ensure good thermalization, the single crystals were fixed with Apiezon grease.

(10) (a) Boskovic, C.; Bircher, R.; Tregenna-Piggott, P. L. W.; Güdel, H. U.; Paulsen, C.; Wernsdorfer, W.; Barra, A.-L.; Khatsko, E.; Neels, A.; Stoeckli-Evans, H. *J. Am. Chem. Soc.* **2003**, *125*, 14046−14058. (b) Yang, E.-C.; Wernsdorfer, W.; Zakharov, L. N.; Karaki, Y.; Yamaguchi, A.; Isidro, R. M.; Lu, G.-D.; Wilson, S. A.; Rheingold, A. L.; Ishimoto, H.; Hendrickson, D. N. *Inorg. Chem.* **2006**, *45*, 529−546.

(11) (a) Lecren, L.; Roubeau, O.; Coulon, C.; Li, Y.-G.; Le Goff, X. F.; Wernsdorfer, W.; Miyasaka, H.; Clérac, R. *J. Am. Chem. Soc.* **2005**, *127*, 17353−17363. (b) Yoo, J.; Wernsdorfer, W.; Yang, E.-C.; Nakano, M.; Rheingold, A. L.; Hendrickson, D. N. *Inorg. Chem.* **2005**, *44*, 3377−3379.

(12) (a) Wernsdorfer, W.; Aliaga-Alcalde, N.; Hendrickson, D. N.; Christou, G. *Nature* **2002**, *416*, 406−409. (b) Tiron, R.; Wernsdorfer, W.; Aliaga-Alcalde, N.; Christou, G. *Phys. Rev. B* **2003**, *68*, 140407(R). (c) Tiron, R.; Wernsdorfer, W.; Foguet-Albiol, D.; Aliaga-Alcalde, N.; Christou, G. *Phys. Rev. Lett.* **2003**, *91*, 227203. (d) Wernsdorfer, W.; Bhaduri, S.; Vinslava, A.; Christou, G. *Phys. Rev. B* **2005**, *72*, 214429.

(13) (a) Miyasaka, H.; Nezu, T.; Sugimoto, K.; Sugiura, K.; Yamashita, M.; Clérac, R. *Inorg. Chem.* **2004**, *43*, 5486−5488. (b) Miyasaka, H.; Clérac, R. *Bull. Chem. Soc. Jpn.* **2005**, *78*, 1725−1748. (c) Kachi-Terajima, C.; Miyasaka, H.; Sugiura, K.; Clérac, R.; Nojiri, H. *Inorg. Chem.* **2006**, *45*, 4381−4390.

(14) Miyasaka, H.; Clérac, R.; Wernsdorfer, W.; Lecren, L.; Bonhomme, C.; Sugiura, K.; Yamashita, M. *Angew. Chem., Int. Ed.* **2004**, *43*, 2801−2805; *Angew. Chem.* **2004**, *116*, 2861−2865.

(15) Lu, Z.; Yuan, M.; Pan, F.; Gao, S.; Zhang, D.; Zhu, D. *Inorg. Chem.* **2006**, *45*, 3538−3548.

(16) Sailaja, S.; Reddy, K. R.; Rajasekharan, M. V.; Hureau, C.; Rivière, E.; Cano, J.; Girerd, J. J. *Inorg. Chem.* **2003**, *42*, 180−186.

(17) Miyasaka, H.; Clérac, R.; Ishii, T.; Chang, H.-C.; Kitagawa, S.; Yamashita, M. *J. Chem. Soc., Dalton Trans.* **2002**, 1528−1534.

(18) Ashmawy, F. M.; McAuliffe, C. A.; Parish, R. V.; Tames, J. *J. Chem. Soc., Dalton. Trans.* **1985**, 1391−1397.

(19) Boudreaux, E. A., Mulay, L. N., Eds. *Theory and Applications of Molecular Paramagnetism*; John Wiley & Sons: New York, 1976.

(20) Wernsdorfer, W. *Adv. Chem. Phys.* **2001**, *118*, 99.

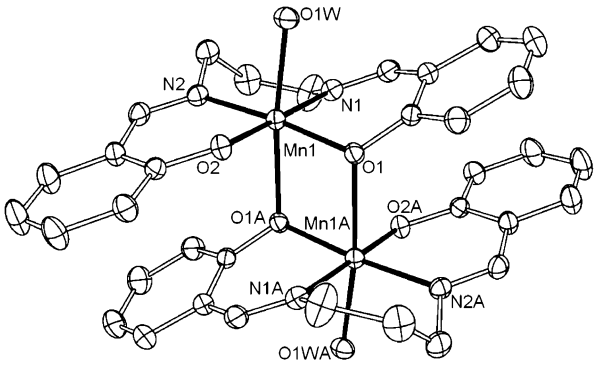

Figure 1. ORTEP drawing of the cationic part of **3** (thermal ellipsoids set at 30%). H atoms and ClO_4^- counter anions were omitted for clarity. Selected bond distances [Å] and angles [deg]: Mn(1)···Mn(1A) 3.258(5), Mn(1)−O(1) 1.9105(2), Mn(1)−O(2) 1.8897(2), Mn(1)−N(1) 2.017(2), Mn(1)−N(2) 1.991(2), Mn(1)−O(1A) 2.3407(2), Mn(1)−O(1W) 2.1890(2), O(1WA)−Mn(1)−O(1) 172.91(7), O(1)−Mn(1)−O(1A) 80.42(7), Mn(1)−O(1)−Mn(1A) 99.58(7) (with #A indicates the $-x, -y + 1, -z$ symmetry operation).

Crystallography. Data collection was performed on a Nonius Kappa CCD diffractometer with a graphite-monochromated Mo Kα radiation ($\lambda = 0.71073$ Å) at 150(2) K. A suitable crystal was affixed on a glass fiber using silicone grease and transferred to the goniostat. DENZO-SMN[21] was used for data integration, and SCALEPACK[21] corrected data, for Lorentz-polarization effects. The structure was solved by direct methods and refined by a full-matrix least-squares method on F^2 using the SHELXTL crystallographic software package.[22] Crystal and experimental data for **3**: $C_{34}H_{36}N_4O_{14}Cl_2Mn_2$, FW = 905.45, monoclinic $C2/c$, $T = 150(2)$ K, $a = 19.890(4)$ Å, $b = 13.460(3)$ Å, $c = 14.700(3)$ Å, $\beta = 110.69(3)°$, $V = 3681.7(13)$ Å^3, $Z = 4$, $D_{calc} = 1.634$ g·cm^{-3}, $F_{000} = 1856$, $2\theta_{max} = 54.9°$. Final $R = 0.0403$ ($I > 2.00\sigma(I)$), $R = 0.0661$ (all data, $R = \sum||F_o| - |F_c||/\sum|F_o|$), wR2 = 0.1087 (all data, wR2 = $[\sum w(F_o^2 - F_c^2)^2/\sum w(F_o^2)^2]^{1/2}$), GOF = 1.034 for 259 parameters and a total of 14182 reflections, 4194 unique ($R_{int} = 0.0486$); equivalent reflections were merged. Maximum positive and negative peaks in ΔF map were found to be $\rho_{max} = 0.355$ e·Å^{-3} and $\rho_{min} = -0.520$ e·Å^{-3}. Crystallographic data have been deposited at the Cambridge Data Centre as supplementary publication no. CCDC-613071.

Results and Discussion

Synthesis and Structural Characterization. Reaction of $Mn(O_2CCH_3)_3{\cdot}4H_2O$ and H_2salpn in methanol at 50 °C followed by addition of $NaClO_4$ with water, yields green crystals of $[Mn_2(salpn)_2(H_2O)_2](ClO_4)_2$ (**3**) within several days (see Experimental Section) suitable for single-crystal X-ray diffraction analysis. This compound crystallizes in the monoclinic $C2/c$ space group with $Z = 4$ and a chemical formula, $[Mn_2(salpn)_2(H_2O)_2](ClO_4)_2$, analogue to **2**.[17] The crystal structure is solely composed of a centrosymmetrical $[Mn_2(salpn)_2(H_2O)_2]^{2+}$ dinuclear part shown in Figure 1 and two ClO_4^- anions that balance the charge. The phenol functions of the Schiff-base ligand have been deprotonated during the synthesis and occupy the equatorial plane of the Mn site (selected bond distances and angles are given in the caption of Figure 1). The out-of-plane Mn axial positions are occupied by a water molecule (O1W) and an oxygen atom (O1A) from the neighboring $[Mn(salpn)]^+$ unit involved in the dinuclear complex. These two Mn−O bond distances are significantly longer than the equatorial bonds as expected for a Jahn−Teller distortion of Mn ions with a +III oxidation state. In the $[Mn_2(salpn)_2(H_2O)_2]^{2+}$ core, the two elongation axes are parallel.

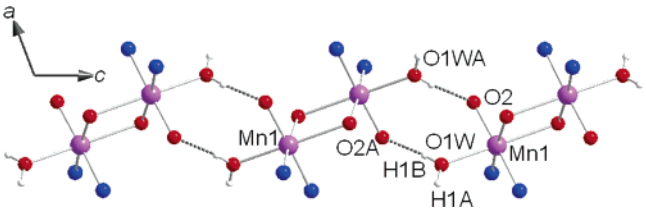

Figure 2. View of the 1D hydrogen-bond network of **3** along the *c*-axis and the formation of a supramolecular chain motif. C and H atoms of the salpn^{2-} ligand and ClO_4^- anions were omitted for clarity.

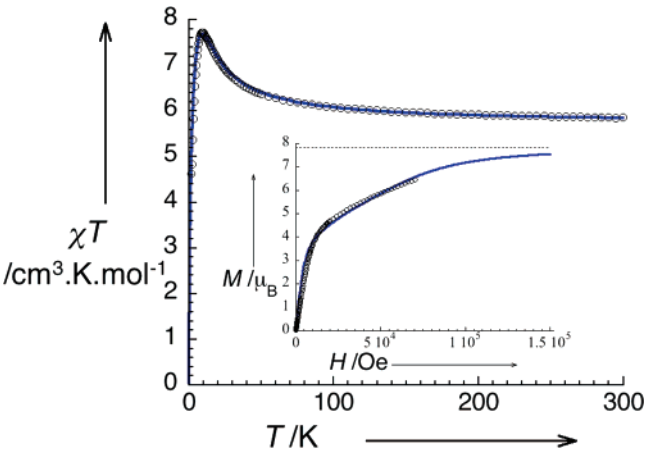

Figure 3. χT vs T plot for **3** (polycrystalline sample) under 1 kOe. (Inset) M vs H plot for **3** at 1.81 K. The blue lines represent the best simulations obtained with the models described in the text.

On the other hand, in the crystal packing, two $[Mn_2(salpn)_2(H_2O)_2]^{2+}$ orientations can be identified and form an angle (α) of 31° between the respective Jahn−Teller axes. The average direction of these two Jahn−Teller orientations is pointing along the c^* axis. As shown in Figure 2, these two different complexes are alternatively connected in one dimension along the *c*-axis through two hydrogen bonds involving O1W from the axial water molecules and O2A from the salpn^{2-} ligand (and by symmetry O1WA and O2) with a short O1W−O2A bond (2.733(2) Å). The ClO_4^- counter anions enfold and isolate the chains, preventing any other type of weak contacts that could mediate magnetic interactions (Figure S1).

Static Magnetic Properties. The magnetic properties of **3** have been investigated. As observed in **1**, the χT product (with $\chi = M/H$) increases gradually from 5.85 cm^3·K·mol^{-1} at 300 K to 7.7 cm^3·K·mol^{-1} at 9 K, highlighting the presence of intradimer ferromagnetic interactions (Figure 3). Below 9 K, χT decreases abruptly to reach 4.63 cm^3·K·mol^{-1} at 1.81 K, suggesting the effect of interdimer antiferromagnetic interactions and/or magnetic anisotropy.

In order to simulate the experimental data, the following spin Hamiltonian has been considered:

$$H = -2J(\mathbf{S}_{Mn1}\cdot\mathbf{S}_{Mn2}) + D_{Mn}(S_{z,Mn1}{}^2 + S_{z,Mn2}{}^2)$$

where J is the intradimer $Mn^{III}-Mn^{III}$ magnetic interaction, D_{Mn} is the zero-field splitting (ZFS) parameter of a single Mn^{III} ion, and $S_{z,Mn}$ is the z component of the $\mathbf{S}_{Mn}$ operators. As already employed for **1**, the magnetic susceptibility was calculated using

(21) Otwinowski, Z.; Minor, W. *Methods Enzymol.* **1997**, *276*, 307−326.
(22) (a) Sheldrick, G. M. *SHELXL97*, Program for Crystal Structure Refinement; University of Göttingen: Germany, 1997. (b) Sheldrick, G. M. *SHELXS97*, Program for Crystal Structure Solution; University of Göttingen: Germany, 1997.

Scheme 2. Schematic View at 0 K and without Applied Field of the Chain Arrangement in the *bc** Plane, Emphasizing the Spin Orientations and Their Resulting Projections along the *c** and *b* Axes, Respectively, the Easy and Intermediate Magnetic Axes of the Crystal

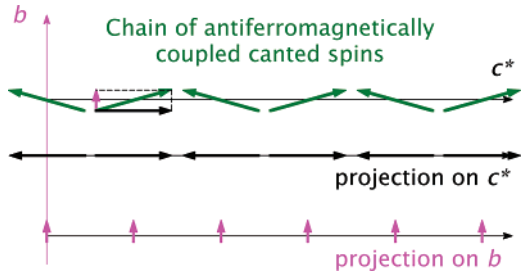

a general procedure (MAGPACK program)[23] including J, D_{Mn}, and g parameters and treating intercomplex interactions (J') in the frame of the mean-field approximation.[14] It is worth mentioning here that J' is likely mediated by the hydrogen bonds described in the structural part, as no other weak contact has been identified between $[Mn_2(salpn)_2(H_2O)_2]^{2+}$ units. In the whole range of temperatures, the experimental data are very well simulated by the above model, in particular below 20 K. The best set of parameters found is $J/k_B = 1.8(1)$ K, $D_{Mn}/k_B = -4.5(2)$ K, $J'/k_B = -0.04(1)$ K and $g = 1.96(1)$ (blue line in Figure 3). The J, D_{Mn}, and g values are typical of this type of dinuclear complex that possesses an $S_T = 4$ ground state.[14,17] Using these parameters, the energy gap created by the zero-field splitting effect, i.e., the anisotropy, on the ground state can be estimated at 26.4 K (Δ_A) (Figure S2), and thus the effective D_{Mn2} for the whole complex should be −1.65 K. The presence of a significant anisotropy is confirmed by the M vs H data at 1.81 K (inset of Figure 3). Indeed at 7 T, the magnetization of the polycrystalline sample is still not completely saturated as expected when the magnetic anisotropy is large. The theoretical magnetization field dependence at 1.81 K calculated from the obtained magnetic parameters (blue line in the inset of Figure 3)[24] agrees well with the experimental data and thus confirms the coherence of the model. At this stage of the magnetic property investigation, the 1D arrangement of $[Mn_2(salpn)_2(H_2O)_2]^{2+}$ units made by the hydrogen bonds (see structural part) can be magnetically viewed at $T = 0$ K as a chain of antiferromagnetically coupled $S_T = 4$ anisotropic spins. For the following discussion, it is also important to keep in mind the presence of two dimer orientations possessing their own anisotropy direction (Jahn−Teller axis) along the chain. Therefore, the spins are indeed canted in the chain arrangement (with a splitting angle, α, of 31° and at ±15° from the *c** axis in the *bc** plane) as shown in Scheme 2.

Slow Relaxation of the Magnetization: Quantum Dynamics Seen by dc Measurements. In order to probe the possible slow relaxation of the magnetization in **3**, measurements below 1.8 K have been performed using a μ-SQUID apparatus. Below 1.4 K, M vs H data measured in the easy direction (*c**) of an oriented crystal (Figure 4) exhibit hysteresis phenomenon (i.e. slow relaxation of the magnetization) with marked steps that become temperature independent below ∼0.5 K. While the *SMM* behavior of the isolated dinuclear $[Mn_2(saltmen)_2]^{2+}$ unit in **1** reveals only one step in zero field (Figure S3) due to fast ground-state *QTM*,[14] three steps at 0 and ±0.32 T ($\pm H_1$) are clearly present for **3** (Figure 4). In many *SMMs*, resonant *QTM* between the ground state and excited m_S levels can be detected on the M vs H data with the observation of regularly spaced steps ($\Delta H = |D_{ST}|/(g\mu_B)$).[1] Due to the presence of two complex orientations in **3**, ΔH becomes $|D_{Mn2}|/(g\mu_B \cos(\alpha/2))$ and can be estimated at 1.3 T based on the above estimation of D_{Mn2} (−1.65 K) and the α angle (31°). Obviously, this value is too large in comparison to H_1 (or $2H_1$) to invoke resonant *QTM* in the explanation of the present features. Therefore, crystal packing effects in their general sense have to be considered in order to understand this peculiar behavior. Indeed, similar steps have also been observed in systems that possess magnetic exchange between *SMM* units.[10,12] Nevertheless, it is noteworthy that such a three-step feature has never been observed in these compounds.

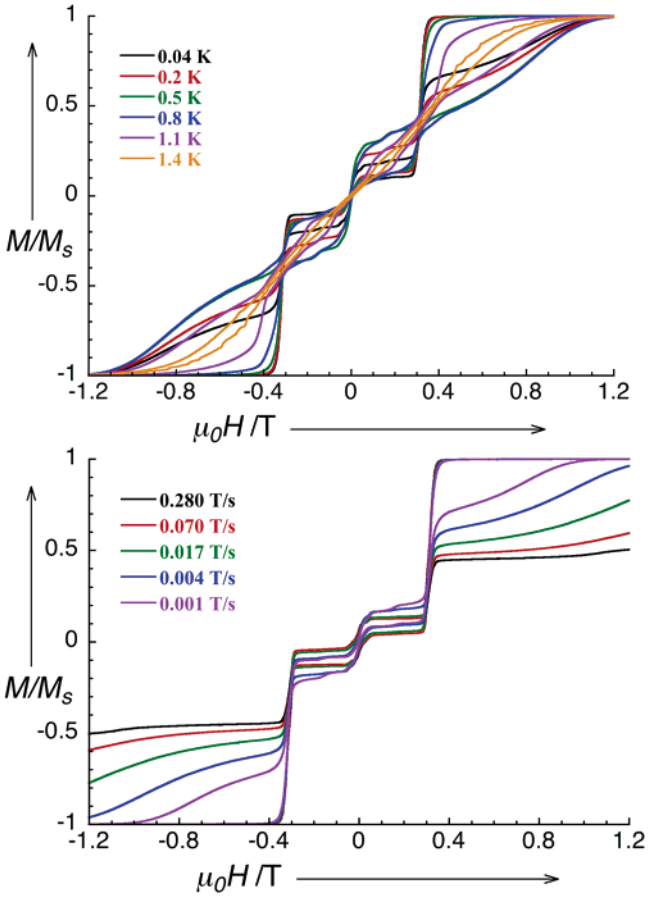

Figure 4. Field dependence of the normalized magnetization performed on an oriented single crystal of **3** at different temperatures with a sweep-field rate of 0.002 T/s (top) and with different sweep-field rate at 0.04 K (bottom). In these experiments, the field was applied in the easy direction of the crystal, i.e., along the *c** axis.

However, the phenomenological model developed for a 3D network of *SMMs* in ref 12b can explain the presence of a step at $-H_1$ with nonvanishing magnetization followed by steps at $H = 0$ and H_1 (Figure 5, red curve) if the 1D arrangement of $[Mn_2(salpn)_2(H_2O)_2]^{2+}$ units (Figure 2) is taken into account.

(23) Borrás-Almenar, J. J.; Clemente-Juan, J. M.; Coronado, E.; Tsukerblat, B. S. *J. Comput. Chem.* **2001**, *22*, 985−991.

(24) The simulation of the M vs H data at 1.8 K has been performed using $J/k_B = 1.8$ K, $D_{Mn}/k_B = -4.5$ K, and $g = 1.96$. It is worth noting that J' has been neglected in the simulation of these data for simplicity and also because its value is too small to change the theoretical curve at high field. Therefore, this simplified model confirms well the amplitude of the J, D_{Mn}, and g parameters. The small theory/experiment discrepancy at low field also supports the presence of J'.

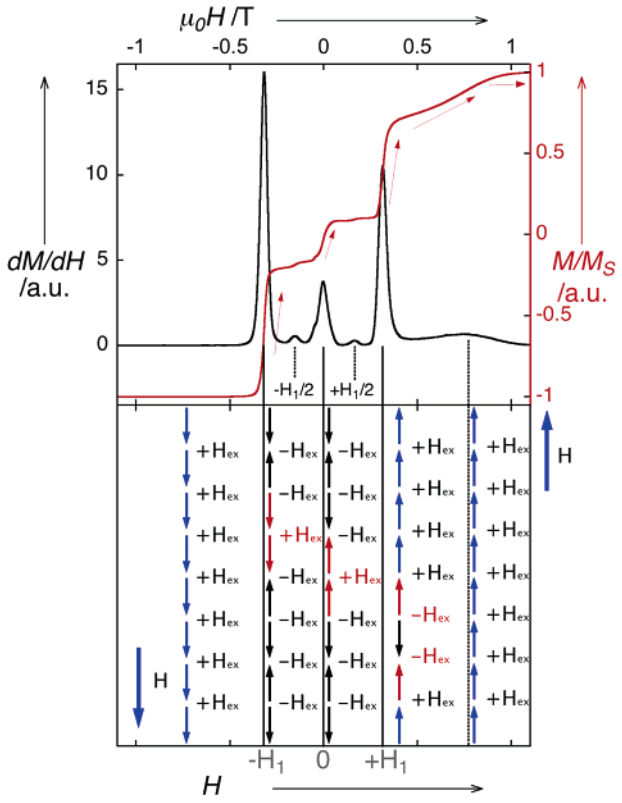

Figure 5. (Top) M/M_S and dM/dH vs H data performed on an oriented single crystal of **3** at 0.04 K with an increasing sweep-field rate of 0.001 T/s (from −1.1 to 1.1 T). (Bottom) Scheme of the spin chain topology illustrating the observed dynamics (with arrows representing the spin projection along the dc field, H, applied in the c^* direction).

In order to understand this approach, it is useful to do a comparison of the magnetization curves reported for both **1** and **3** (Figures S3 and 4, respectively). For **1**, at a strong enough negative field only the $m_S = -4$ level of the $S_T = 4$ ground state is populated. As the field is increased, this state remains the lowest energy one until $H = 0$, at which point the two $m_S = \pm 4$ states have the same energy. At zero field, two important events occur: (i) as the probability to be either in the $m_S = +4$ or in the $m_S = -4$ state is the same, the equilibrium magnetization is zero even in the $T = 0$ K limit; and (ii) the population between the two $m_S = \pm 4$ states is equilibrated through *QTM*. The data shown in Figure S3 have been well understood in these terms as described in ref 14.

Coming back to **3**, each elementary magnetic unit composing the chain experiences an effective magnetic field that results from the applied field (H) and the exchange fields ($\sum H_{ex}$) created by magnetic interactions with its neighbors: $H_{eff} = H + \sum H_{ex}$. When applying a strong negative dc field to the system, the spin projections on the c^* axis (Scheme 2) are all aligned along the field direction (*S configuration*, blue spins, Figure 5). A similar situation observed for **1** at $H = 0$ is now found at $H = -H_1$ (with $H_1 = 2H_{ex} = 0.32$ T), when each spin experiences an effective zero field and thus can flip by *QTM*. Nevertheless, in order to understand the peculiar magnetic behavior of **3** in detail (Figures 4 and 5), it is not enough to look at the dynamic properties of a single spin unit even at $H = -H_1$, but it is absolutely necessary to extend the view to the whole chain in which these spins are connected through magnetic interactions. Considering that at a temperature low enough only the $m_S = \pm 4$ states of each dinuclear unit are significantly populated, this system can be described as a chain of N Ising $S_T = 4$ spins and with the following Hamiltonian:

$$H = -2J'S_T^2 \cos(\alpha) \sum_{i=1}^{N} \sigma_i\sigma_{i+1} - g\mu_B HS_T \cos(\alpha/2) \sum_{i=1}^{N} \sigma_i$$

or using the exchange field H_{ex} defined above:

$$H = g\mu_B S_T \cos(\alpha/2)[H_{ex} \sum_{i=1}^{N} \sigma_i\sigma_{i+1} - H \sum_{i=1}^{N} \sigma_i]$$

The lowest-lying configurations of a given magnetization along the chain easy axis c^*, $M_r = g\mu_B S_T \cos(\alpha/2)(N - 2r)$, can be labeled by means of an integer r with $0 \le r \le n$ with $n = N/2$. Starting from the saturation case (*S configuration*, $r = 0$), the first excited states are obtained, reversing every second spin. This mechanism implies a reduction of the exchange energy (considering that $J' < 0$) and an increase of the Zeeman term in the presence of an external field. For the flip of a spin having two neighbors in the chain, the energy difference with respect to the saturated configuration ($r = 0$) is $\Delta E_r = g\mu_B S_T^2 \cos(\alpha/2)(-4H_{ex} + 2|H|)r$. The number of excited configurations Ω_r corresponding to a given M_r magnetization is obtained by the binomial coefficient: $\Omega_r = {}_nC_r = n!/(r!(n - r)!)$. This coefficient is maximum for $r = n/2$, which can be approximated using the Stirling's formula as:

$$\Omega_{n/2} = {}_nC_{n/2} \approx \left\{2^n \frac{\sqrt{2}}{\sqrt{n\pi}}\right\}$$

The *AF* ground state ($r = n$, $M_r = 0$) and the saturated configuration ($r = 0$, $M_{sat} = Ng\mu_B S_T \cos(\alpha/2)$) are thus separated by an ***exponentially*** large number of chain states with intermediate magnetization. It is worthwhile to note that this phenomenological argument applies only to relatively long (N) arrays of antiferromagnetically coupled magnetic units, thus marking a substantial difference between the present system and usual *SMMs*.

Therefore at $H = -H_1$, ***all*** the lowest-energy chain states possess the same energy ($\Delta E_r = 0$) inducing some substantial differences in the relaxation process in comparison to what occurs for **1** at $H = 0$. In spite of the fact that for fields $-H_1 < H < 0$ the lowest-energy state should be an antiferromagnetic *configuration* (*AF configuration*, black spins, Figure 5), this latter is, in practice, never attained at low temperature. In fact, exactly at $H = -H_1$, *QTM* of individual spin units allows the system more likely to go from the *S configuration* to one of the many other states labeled by r. As soon as *QTM* is not effective ($-H_1 < H < 0$), the system remains "trapped" in one of these states (schemes of Figure 5). In Figure 4, one can appreciate how this trapping effect is more and more pronounced as the temperature is lowered (Figure 4, top) or the field sweep rate is increased (Figure 4, bottom). It is important to comment that at $H = -H_1$ all the chain excited states have negative magnetization, whereas the *AF* configuration possesses a zero magnetization. This situation induces at $H = -H_1$ that the magnetization expected for $T = 0$ K is not zero but rather an intermediate value between $-M_{sat}$ and zero. Therefore, as observed experimentally, the magnetization at $H = -H_1$, where *QTM* occurs, is not directly jumping from the negative saturated

magnetization to zero as in the case of the isolated dinuclear complex **1** at $H = 0$.

In the chain excited states trapped at $H = -H_1$, while most of the spin projections are antiferromagnetically arranged, some spin units experience a total exchange field, $\sum H_{ex}$, equal to zero (red spins in Figure 5). Hence at $H = 0$, *QTM* can occur for these spins. Consequently, for a chain state with a given magnetization, there is always another state with opposite magnetization which is equally populated (being connected by *QTM*). Once this scenario is established, even if a residual nonequilibrium population of the excited states is present, a vanishing magnetization is actually observed at $H = 0$.

When H reaches H_1, the field can overcome the interdimer antiferromagnetic interactions and thus tries to align all the σ_i spins along its direction. Above H_1 and likewise between $-H_1$ and H_1, some spins stay trapped in one of the numerous chain exited states, preventing a direct saturation of the magnetization. Nevertheless, at higher fields around 1.2 T, these trapped spins finally align with the field due to direct relaxation processes and spin−spin cross-relaxation.[10,25] As one expects, the same sequence of phenomena, but associated with opposite magnetization, is obtained while H is decreased, starting from positive large fields.

From this phenomenological description, it is also possible to estimate the magnetic interaction between $[Mn_2(salpn)_2(H_2O)_2]^{2+}$ units considering that at $H = \pm H_1$ the Zeeman and the exchange energies are equal:

$$g\mu_B S_T H_1 \cos(\alpha/2) = 4|J'|S_T^2 \cos(\alpha) \quad \text{(i.e., } H_1 = 2H_{ex}\text{)}$$

Hence, from $H_1 = 0.32$ T, J' can be estimated at -0.03 K in good agreement with the estimated value from the χT vs T simulation (Figure 3).

In Figure 5, additional minor steps are observed at $\pm H_1/2$ (± 0.16 T). These fields could correspond to the quantum relaxation of complexes under the influence of only one instead of two exchange fields ($H_1/2 = H_{ex}$). Therefore, the simplest way to explain the presence of these half-field steps is to invoke the presence of finite-sized chains and the reversal of the spins occupying the end of opened chains. The flip of one ending spin in one of the trapped chain states (all with negative magnetization for $-H_1 < H < 0$) brings an energy change of $\Delta E = g\mu_B S_T \cos(\alpha/2)(-2H_{ex} + 2|H|)$ and also a variation of the magnetization. Therefore, a relatively small step is actually expected at a field equal to $H_1/2$. In practice, the relative magnitude of this jump is to be compared with the average length of the chains in the system, which is inversely proportional to the probability of having a defect breaking the chains. The typical lengths estimated for these kinds of compounds[6,11a] are consistent with the observation of a 2% (of the saturated magnetization) jump at half of the field where the major step occurs. Therefore the chain length in **3** can be estimated roughly at about 100 units.

Slow Relaxation of the Magnetization: Thermally Activated Relaxation Seen by ac Measurements. The slow relaxation of the magnetization observed on the M vs H plots has also been studied using the ac technique above 1.8 K. At zero dc field, a frequency-dependent out-of-phase ac signal is detected below 5 K for frequencies ranging from 1 to 1500 Hz (Figure 6, top). The relaxation time (τ) of **3** deduced from these measurements follows a thermally activated behavior (Arrhenius law, Figure 7): $\tau = \tau_0 \exp(\Delta_{eff}/T)$ with the following parameters: $\tau_0 = 6.5 \times 10^{-7}$ s and $\Delta_{eff} = 15.5$ K. As expected, due to the presence of zero-field *QTM* (see Figures 4 and 5), the obtained energy barrier is lower than the estimated theoretical gap (vide supra, $\Delta_A = 26.4$ K). Therefore, in order to suppress the quantum relaxation pathway, τ was measured under dc fields. When H increases, the characteristic frequency at 2.4 K decreases from 330 Hz at $H = 0$ Oe to about 20 Hz at 1500 Oe (Figure 8). Then this value increases slowly to reach 33 Hz at 0.5 T. The relaxation time measured at 1500 Oe (field at which τ is the smallest, Figure 8) follows a new Arrhenius law (Figure 7) with $\tau_0 = 2 \times 10^{-8}$ s and $\Delta_{eff} = 31.0$ K.

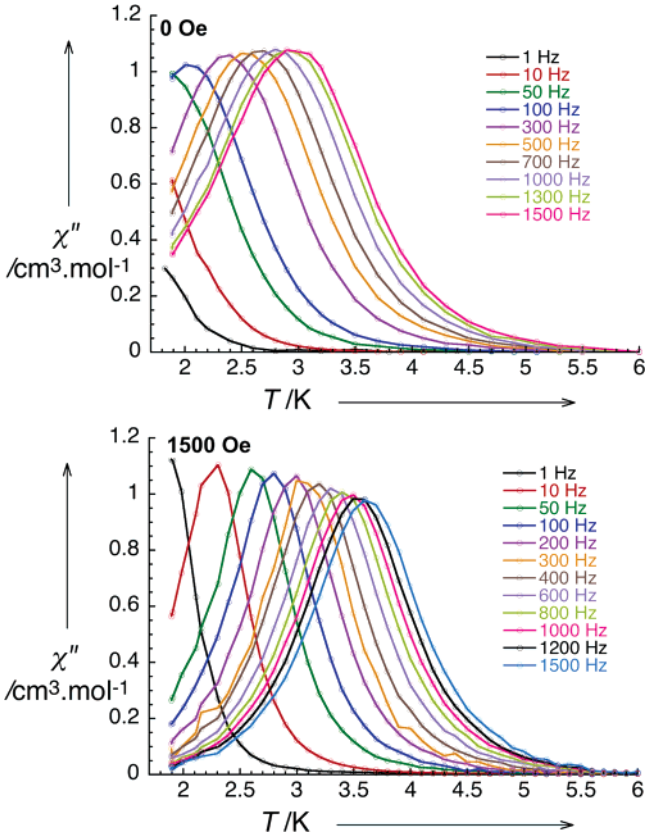

Figure 6. χ'' vs T data for ac frequencies ranging from 1 to 1500 Hz performed at zero dc field (top) and at 1500 Oe (bottom) on a polycrystalline sample of **3**.

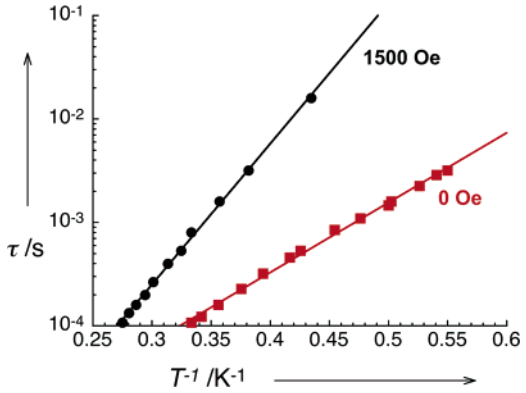

Figure 7. τ vs T^{-1} plot obtained at 0 and 1500 Oe dc fields.

(25) Wernsdorfer, W.; Bhaduri, S.; Tiron, R.; Hendrickson, D. N.; Christou, G. *Phys. Rev. Lett.* **2002**, *89*, 197201.

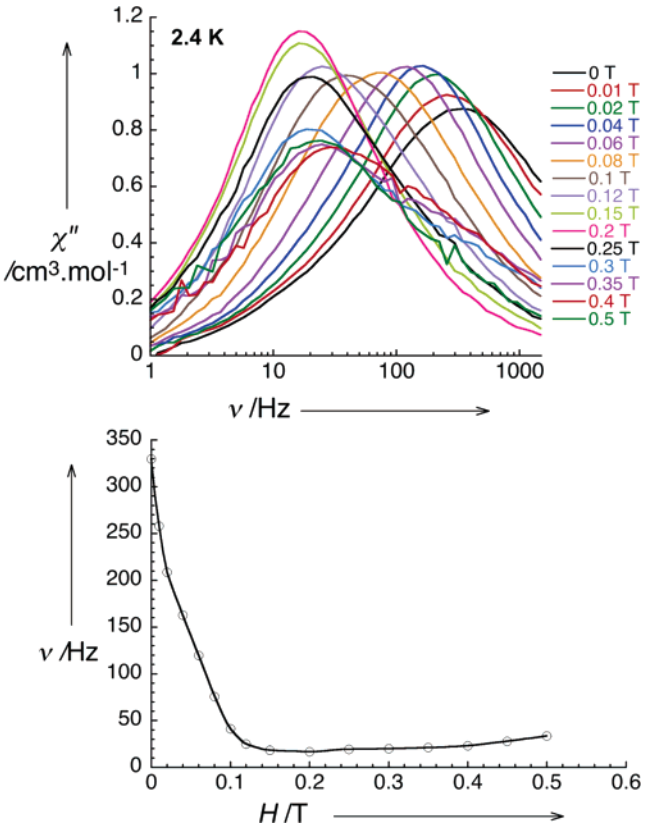

Figure 8. (Top) Frequency dependence of the out-of-phase susceptibility performed on a polycrystalline sample of **3** at 2.4 K with different dc fields. (Bottom) Field dependence of the characteristic frequency at 2.4 K deduced from the χ'' vs ν plot given on the right.

As previously observed in *SCM* systems[4−6] and in chains of ferro- or antiferromagnetically coupled *SMMs*[4,11a] the observed dynamics should be modified by the intrachain magnetic interactions. Applying the approach described in refs 4 and 11a to the present supramolecular chain of canted antiferromagnetically coupled *SMMs*, the energy gap of the relaxation time should be $\Delta_\tau = 2\Delta_\xi + \Delta_A$ within the Ising limit:

$$\Delta_A = |D_{Mn2}|S_T^2/k_B \quad \text{and} \quad \Delta_\xi = 4|J'|S_T^2\cos(\alpha)/k_B$$

Using $D_{Mn2}/k_B = -1.65$ K and $J'/k_B = -0.03$ K, Δ_τ should thus be equal to 29.7 K ($\Delta_A = 26.4$ K and $\Delta_\xi = 1.65$ K) in excellent agreement with the experimental energy gap ($\Delta_{eff} = 31$ K). As already shown at low temperature for the quantum relaxation in the previous paragraph, the thermal relaxation regime of **3** is not the one of a usual *SMM*. Indeed, the magnetic interactions along the 1D organization of $[Mn_2(salpn)_2(H_2O)_2]^{2+}$ modulate the pristine behavior expected for isolated *SMM* complexes as, for example, in **1**.[14] As shown here, the intercomplex interactions induce a magnetic "link" between *SMM* units, increasing the energy gap of relaxation (Δ_τ), thus slowing down the thermal dynamics.

Concluding Remarks

In summary, the present compound contains 1D hydrogen-bonded organization of *SMM* units that is well isolated in the crystal packing. For the first time, the intricate slow relaxation of the magnetization in such supramolecular arrangement has been observed and described at the frontier of *SMM* and *SCM* behaviors. Unique quantum and thermally activated dynamics have been detected and rationalized on the basis of the known *SMM* behavior of dinuclear Mn^{III}/salen-type complexes[14] and the presence of weak 1D interactions between these types of units. Below 0.5 K, multiple steps on the *M* vs *H* data have been attributed to the ground-state quantum tunneling of the magnetization shifted (at $H = \pm H_1$) by the intrachain exchange interactions and revealed in zero field by the presence of trapped "chain excited states". Moreover, the impact of the one-dimensionality on the quantum dynamics is also proved by the observation of finite-sized chain effects that allow a separated detection of the ending spins quantum dynamics (at $H = \pm H_1/2$). Above 1.8 K, the thermally activated regime of **3** has been studied in zero field and also in a small dc field in order to prevent the quantum tunneling pathway of relaxation. Its characteristic relaxation time follows an activated behavior with an energy gap ($\Delta_{eff} = 31.0$ K) that can be understood by applying the relaxation approach used for Ising-type *SCM* systems ($\Delta_\tau = 2\Delta_\xi + \Delta_A = 29.7$ K). If the thermally activated relaxation of $[Mn_2(salpn)_2(H_2O)_2](ClO_4)_2$ is very similar to the one observed in *SCMs* and related 1D systems,[4−7,11] the presence of magnetization quantum tunneling clearly indicates that the observed behavior originates from a molecular origin and the *SMM* properties of the $[Mn_2(salpn)_2(H_2O)_2]^{2+}$ unit. Following the denomination used by Wernsdorfer et al.,[12] this system could be qualified as a "one-dimensional exchange-coupled *SMM*". Finally, this work illustrates nicely that the quantum and thermally activated relaxations of a *SMM* can be tuned and modulated by playing at the molecular level on supramolecular interactions and their organization.

Acknowledgment. This work was supported by MAGMANet (NMP3-CT-2005-515767), Bordeaux 1 University, the CNRS, the Region Aquitaine, the French Ministries of Foreign Affairs and of Research and the EC-TMR Network "QuEMolNa" (MRTN-CT-2003-504880).

Supporting Information Available: Crystallographic data (CIF); crystal structure packing and additional magnetic measurements. This material is available free of charge via the Internet at http://pubs.acs.org.

JA067744I